

University of Dundee

## Effects of the bottom slope and guiding wall length on the performance of a vortex drop inlet

Rhee, Dong Sop; Park, Yong Sung; Park, Inhwan

*Published in:*  
Water Science and Technology

*DOI:*  
[10.2166/wst.2018.397](https://doi.org/10.2166/wst.2018.397)

*Publication date:*  
2018

*Document Version*  
Peer reviewed version

[Link to publication in Discovery Research Portal](#)

*Citation for published version (APA):*  
Rhee, D. S., Park, Y. S., & Park, I. (2018). Effects of the bottom slope and guiding wall length on the performance of a vortex drop inlet. *Water Science and Technology*, 78(6), 1287-1295.  
<https://doi.org/10.2166/wst.2018.397>

### General rights

Copyright and moral rights for the publications made accessible in Discovery Research Portal are retained by the authors and/or other copyright owners and it is a condition of accessing publications that users recognise and abide by the legal requirements associated with these rights.

- Users may download and print one copy of any publication from Discovery Research Portal for the purpose of private study or research.
- You may not further distribute the material or use it for any profit-making activity or commercial gain.
- You may freely distribute the URL identifying the publication in the public portal.

### Take down policy

If you believe that this document breaches copyright please contact us providing details, and we will remove access to the work immediately and investigate your claim.



27 slope.

28

29 **Keywords:** choking, guiding wall, longitudinal bottom slope, radial bottom slope, vortex drop inlet

30

## 31 **Introduction**

32

33 The types of manholes can be classified as plunging flow drops and vortex drops (Jain 1984). As the name  
34 implies, in a vortex drop, the flow enters through the approach channel and forms a vortex or spiral along the  
35 circular wall of the shaft as it travels downward; in a plunging flow drop, a jet flow occurs (Rajaratnam et al. 1997;  
36 Banisoltan et al. 2015). The vortex flow in the vertical shaft leads to entrain air, which pushes down odors to the  
37 underground space (Motzet & Valentin 2002) and to dissipate flow energy by friction while flowing down the wall  
38 of the vertical shaft (Zhao et al. 2006; Del Giudice et al. 2010). For these reasons, vortex drops are preferred in the  
39 aspects of efficient conveyance and significant energy dissipation (Hager 1985). In general, the inlet of the vertical  
40 shaft can have a screw (Drioli 1947), tangential (Jain & Kennedy 1983), or spiral (Kellenberger 1988) shape, based  
41 on the properties of the approaching flow (see Appendix 1). However, despite the advantages of vortex drops, they  
42 have a relatively high cost due to geometrical complexities, and possible flow patterns disturbing stable flow  
43 conveyance (e.g., standing wave and choking in the intake structure) are obstacles to using vortex drops. Therefore,  
44 reasonable design guidelines to increase the efficiency of vortex drops are necessary.

45 The flow properties in the intake structure of vortex drops have been studied for optimal design. For the  
46 case of a spiral inlet, Quick (1990) published a study of head-discharge relationships to find an efficient design for  
47 intake structures. Hager (1990) reported a theoretical formula for the free surface profile of a standing wave along  
48 the intake wall for a supercritical approaching flow. In consideration of the relatively high cost of a spiral inlet,  
49 Motzet & Valentin (2002) tested a supercritical flow in a screw shaped intake structure, which was originally  
50 intended to convey a subcritical flow, and concluded that the screw inlet could still be used in the case of a  
51 supercritical approaching flow, although the energy dissipation decreases. Subsequently, Del Giudice et al. (2010)  
52 and Del Giudice & Gisonni (2011) proposed a new design criterion for the screw intake structure to be applied in  
53 both in subcritical and supercritical flows. Furthermore, Mulligan et al. (2016) presented an empirical formula for

54 the discharge in a strong free-surface vortex flow to design a screw intake structure. Previous experimental studies  
55 were primarily focused on screw or tangential intake structures for a subcritical approaching flow. However, in  
56 many situations, a supercritical flow commonly occurs at the entrance of the vertical shaft. Thus, the geometry for  
57 the vortex drop shaft with a spiral intake must be tested under several design conditions.

58 The primary objective of the inlet is to achieve a high-volume flow rate with a minimal increase in the  
59 upstream water depth. However, there are at least two important factors to be considered in designing and evaluating  
60 the efficiency of a vortex drop inlet. One factor is the possibility of choking leaving no space for air to escape.  
61 Choking often results in a significant decrease in conveyance and explosive bursts of air, with associated safety  
62 issues; therefore, a vortex drop inlet must be designed such that choking events are prevented. To ensure that there is  
63 adequate passage for air flow at the centre of the vertical shaft, especially for a supercritical approaching flow, an  
64 intake structure consisting of a steep channel with an inner guiding wall could be fitted near the entrance of the  
65 vertical shaft. In addition, it is well-known that a standing wave can form during high-speed flow in a curved  
66 channel (e.g. Ippen, 1943); therefore, the maximum water surface elevation may occur at the crest of a standing  
67 wave located within the inlet structure (Wu et al. 2017). This possibility is the other factor to be considered in the  
68 design of an inlet structure. Based on physical model tests, Hager (1990; 2010) provided a guideline for the inlet  
69 structure geometries, optimizing the height of the standing wave and preventing choking for approaching flows with  
70 a high Froude number.

71 In the present research, we build upon the guidelines for spiral intake structures in conditions of subcritical  
72 and transcritical flows and further investigate the effects of the bottom slope and the guiding wall. In particular, two  
73 types of bottom slope configurations are used: (i) longitudinal slope only and (ii) both longitudinal and radial slopes.  
74 For both types, the length of the inner guiding wall was varied, and the performance was assessed in terms of the  
75 water surface elevation at the junction between the approach channel and the vertical shaft as well as in terms of the  
76 height of the standing wave, if a standing wave occurred. It is shown that a radial slope effectively eliminates the  
77 standing wave, even for a large flow rate.

78

## 79 **Methods**

80

81 We focus on the spiral vortex drop, which is designed for a supercritical flow, and additional design

82 parameters are investigated for subcritical and transcritical approach flows. For the design of the vortex drop intake,  
 83 Hager (1990; 2010) recommended the design parameters as shown in Appendix 1(b), where  $R_1$ ,  $R_2$ ,  $R_3$ , and  $R_4$   
 84 are the radii of the inlet structure;  $R$  is the radius of the vertical shaft;  $a$  is the horizontal distance from the outer  
 85 wall of the approach channel to the centre of the vertical shaft;  $b$  is the width of the approach channel;  $d$  is the  
 86 width of the channel opposite the inlet section; and  $s$  is the thickness of the wall opposite the inlet section;  $s_1$  is  
 87 the thickness of the inlet section;  $e_1$ ,  $e_2$ ,  $e_3$ , and  $e_4$  are the eccentricities of the circular arc constituting the  
 88 inlet structure;  $S_{oo}$  is the bottom slope of the spiral intake.

89 As mentioned in the previous section, the maximum water surface elevation measured from the start of the  
 90 spiral intake,  $h_M$ , may occur within the intake structure because of the standing wave. An empirical equation for  
 91  $h_M$  in terms of the inlet geometric parameters and discharge was given by Hager (1990; 2010) who derived the  
 92 equation for supercritical flow as follows:

93

$$94 \quad \frac{h_M}{R_1} = \left[ \left( \frac{2}{gbh_0R_1^3} \right)^{1/2} Q - \frac{1}{2}S_{oo} \right] (1.1 + 0.15F_0) \quad (1)$$

95

96 in which  $Q$  is the discharge,  $g$  is the gravitational acceleration,  $h_0$  is the water depth at the start of the intake,  
 97 and  $F_0$  is the Froude number at the same location defined as

98

$$99 \quad F_0 = \frac{Q}{\sqrt{gb^2h_0^3}} \quad (2)$$

100

101 The design of inlet structure should be determined to minimize  $h_M$  for the efficient drainage of stormwater. In  
 102 this study,  $h_M$  was measured for both longitudinal and radial slopes.

103 Experiments were conducted at the River Hydraulics Laboratory of the Korea Institute of Civil Engineering  
 104 and Building Technology (KICT). The experimental apparatus is depicted in Figure 1, in which the approach

105 channel (0.6 m long, 0.2 m wide, 0.6 m high) and the vertical shaft with a spiral intake structure ( $a = 0.30$  m,  
 106  $s = 0.01$  m,  $d = 0.10$  m,  $R_1 = 0.25$  m,  $R_2 = 0.15$  m,  $R_3 = 0.09$  m,  $R_4 = 0.10$  m, and  $R = 0.09$  m) were  
 107 built of clear acrylic. Flow was supplied from the high-elevation tank at the beginning of the approach channel. The  
 108 discharged water is eventually collected at the basin underneath the vertical shaft and then recirculated through a  
 109 submerged pump. The spiral intake structure was designed according to the design criteria presented by Hager (1990;  
 110 2010) who proposed the design parameters for a supercritical flow. Figure 1b) shows the details of the intake  
 111 structure, in which the spiral inlet has the longitudinal ( $S_{oo}$ ) and radial bottom slopes ( $S_{oe}$ ). In this channel,  $S_{oo}$   
 112 and  $S_{oe}$  were changed to assess the drainage efficiency in conditions of subcritical and transcritical flows.  
 113 Furthermore, the length of the guiding wall was manipulated by varying the angle,  $\theta$ .

114  
 Figure 1 Descriptions of the experimental apparatus

115  
 116 A total of six different intake structures were built with different bottom slope configurations of the spiral  
 117 intake. Four of the structures had only longitudinal slopes ( $S_{oo} = 5.0\%$ ,  $7.5\%$ ,  $10.0\%$ , and  $12.5\%$ ), and the other two  
 118 had both longitudinal and radial slopes ( $S_{oo} = 5\%$  and  $10\%$  with  $S_{oe} = 5\%$ ). For each of the six spiral intakes, the  
 119 water surface elevation was measured at each measurement sections as shown in Figure 1b) using both a  
 120 capacitance-type wave gauge, which has  $\pm 0.3\%$  error, and tape rulers attached to the vertical shaft (see Appendix  
 121 2). For each spiral intake with different bottom slopes, measurements were repeated as varying the length of the  
 122 guiding wall ( $\theta = 0^\circ, 30^\circ, 60^\circ, 90^\circ, 120^\circ, 150^\circ, 180^\circ, 210^\circ$  and  $270^\circ$ ). In this experimental apparatus, discharge  
 123 ( $0.002 \leq Q \leq 0.030 \text{ m}^3/\text{s}$ ) was varied and the flow changed from the weakly subcritical to the transitional flow  
 124 ( $0.117 \leq F_0 \leq 1.247$ ) according to the hydraulic and geometric conditions. The aforementioned experimental  
 125 conditions are listed in Table 1.

126  
 Table 1 Summary of the experimental conditions

127  
 128 **Results and discussion**

129

130 In this section, we present three sets of analysed data that are directly relevant to the performance of the  
131 vortex drop inlet: (i) water surface elevation–discharge relations, i.e.,  $h_0$  as a function of  $Q$  for each case; (ii)  
132  $h_M/h_0$  as a function of  $Q$  for each case; and (iii)  $F_0$  as a function of  $Q$  for each case. Additionally, we remark  
133 here that both  $h_0$  and  $Q$  are expressed in terms of dimensionless variables defined as follows (Hager 1990;  
134 Hager 2010):

135

$$136 \quad y = \frac{bh_0}{aR} \quad (3)$$

$$137 \quad q = Q \sqrt{\frac{b}{gaR^5}} \quad (4)$$

138

#### 139 *Water surface elevation change by bottom slopes*

140

141 Figure 2 shows the water surface elevation changes observed along the inside of the intake structure. The  
142 figure reveals that the water surface elevation ( $h$ ) rises with increasing discharge ( $Q$ ). In Figure 2a), which shows  
143 the results for only a longitudinal bottom slope ( $S_{00} = 10\%$ ), standing waves are clearly visible (section no. 2-4)  
144 and result in 9.9%-38.9% higher water surface elevation ( $h_M$ ) within the intake structure where is between the  
145 section no. 2 and no. 4 than the water surface elevation at the beginning of the inlet ( $h_0$ ). Furthermore, two local  
146 maximum water surface elevations were observed as reported by Hager (1990) and Crispino et al. (2016) in  
147 conditions of supercritical flow even though the hydraulic conditions in this measurements show subcritical and  
148 transcritical flows. After that, the local maximum water surface elevation was reduced along the spiral inlet due to  
149 subcritical and transcritical inflow conditions. In contrast, in Figure 2b),  $h_M$  is only 0.1%-0.7% higher than  $h_0$   
150 in subcritical flow even though  $h_M$  is located at the section no. 2. In conditions of transcritical flow,  $h_0$  is higher  
151 than the water surface elevation in the inlet structure except the results for  $F_0 = 1.088$  in which  $h_M$  is 2.6%  
152 higher than  $h_0$ . These results show that  $h_M$  can decrease in the inlet structure by adding radial bottom slope.

153

Figure 2 Experimental results for water surface elevations measured at intervals from the start of the spiral intake

154

155 The dimensionless water surface elevation at the beginning of the spiral intake ( $y$ ) is plotted as a function  
156 of the dimensionless discharge ( $q$ ) for varying longitudinal bottom slopes ( $S_{oo}$ ) in Figure 3. The dimensionless  
157 critical depth, which is calculated by replacing  $h_0$  to the critical depth, is also plotted in Figure 3 using a  
158 dashed line. For all cases, the guiding wall managed to prevent choking in the vertical shaft. However, as the extent  
159 of the guiding wall increases, more space is taken up by the wall, leaving less room for flow. As a result,  $y$   
160 increases not only with  $q$  but also with  $\theta$ , which results in a rapid increase of  $y$  with increasing  $q$ .  
161 Furthermore, the flow shown in Figures 3b)-3d) changes from a transcritical to a subcritical flow as increasing  $q$ .  
162 As the longitudinal bottom slope increases from 5.0% to 10.0% (Figures 3a) – 3c)), the adverse effects of the  
163 guiding wall are minimized, and there is a negligible difference between cases with different extents of the guiding  
164 wall when the bottom slope is 10.0%. However, for the case with a steeper slope (12.5%, Figure 3d)), the  
165 performance deteriorates again. Thus, the results suggest that there exists an optimal longitudinal bottom slope.

166

Figure 3  $y$  as a function of  $q$  for the case with a longitudinal slope

167

168 The effects of the radial bottom slope ( $S_{oe}$ ) can be observed by comparing Figures 3a) and 4a) as well as  
169 Figures 3c) and 4b). For the cases with a 5% longitudinal bottom slope, the radial slope (Figure 4a) leads to  
170 0.1%-11.6% decrease over the case without a radial slope (Figure 3a) for  $\theta \geq 180^\circ$ . In contrast, the effect of the 5%  
171 radial bottom slope is significantly improved for the cases with a steeper (10%) longitudinal bottom slope, in which  
172  $y$  decreases 11.2%-12.0% for  $\theta \geq 180^\circ$ .

173

Figure 4  $y$  as a function of  $q$  for cases with longitudinal and radial slopes

174

175 *The maximum water surface elevation in the inlet structure*

176



177 The maximum water surface elevation in the inlet structure is one of the key parameters in designing vortex  
 178 drop inlets. As mentioned previously, with the addition of a spiral intake structure and a guiding wall, the maximum  
 179 water surface elevation may occur downstream from the beginning of the intake even though subcritical or  
 180 transcritical flows occurred at the spiral inlet. Therefore, the maximum water surface elevation within the spiral  
 181 intake ( $h_M$ ) measured from the junction of the inlet channel and the spiral intake relative to the water surface  
 182 elevation at the junction ( $h_0$ ) is expressed as a function of  $q$  in Figures 5 and 6. For each case,  $h_M/h_0$  increases  
 183 as the extent of the guiding wall decreases, primarily because  $h_0$  or  $y$  increases as the extent of the guiding wall  
 184 increases, as shown previously in Figure 3. However,  $h_M/h_0$  does not show monotonic behaviour with respect to  
 185  $q$ , in contrast with the monotonic tendency of  $y$  in Figure 3; instead, it either maintains an approximately  
 186 constant value (Figures 5a), 6a) and 6b)) or increases initially and later decreases from a maximum to a constant  
 187 value (Figures 5b), 5c) and 5d)). Interestingly, in these latter cases, the increased longitudinal bottom slope  
 188 effectively reduced  $y$ . Therefore, it is reiterated once again that  $h_M$  is also an important design parameter.

189

Figure 5  $h_M/h_0$  as a function of  $q$  for the case with a longitudinal slope

190

Figure 6  $h_M/h_0$  as function of  $q$  for cases with longitudinal and radial slopes

191

192 This rather complicated behaviour of  $h_M/h_0$  can be explained in terms of the Froude numbers defined in  
 193 Eq. (14), which are plotted in Figures 7 and 8. First, the two cases with a 5.0% longitudinal bottom slope (Figures 7a)  
 194 and 8a)) maintain a subcritical flow under all experimental conditions, and the maximum elevation occurs at the  
 195 beginning of the spiral intake. By comparing Figures 7b), 7c) and 7d) to the corresponding Figures 5b), 5c) and 5d),  
 196 it is observed that  $h_M/h_0$  is greater than one for subcritical and transcritical flows. With a further increase of  $q$ ,  
 197 the water depth goes beyond the critical value, and the flow becomes subcritical as shown in Figures 3 and 4, while  
 198  $h_M/h_0$  decreases to a constant value.

199

Figure 7  $F_0$  as a function of  $q$  for the case with a longitudinal slope

200

Figure 8  $F_0$  as a function of  $q$  for cases with longitudinal and radial slopes

201

202 The experimental result for the spiral intake with both a 10.0% longitudinal bottom slope and a 5.0% radial  
203 slope (Figure 8b)) is quite interesting. Except for the case with a  $270^\circ$  guiding wall, which consistently shows a  
204 subcritical flow, the flows are, in general, trans-critical. Unlike the previous observation illustrated in Figures 5b), 5c)  
205 and 5d), this case maintains  $h_M/h_0 \approx 1$  for all discharge conditions, similar to the cases with a subcritical flows,  
206 because the radial slope shifts the hydraulic jump further downstream in the spiral intake (see Figure 2). The average  
207 values of  $y$  and  $h_M/h_0$  ( $\bar{y}$  and  $\overline{h_M/h_0}$ ) are compared in Table 2 based on the radial bottom slope. The  
208 difference ( $\varepsilon$ ) between the two observations was calculated as follows:

209

$$\varepsilon = \frac{1}{n} \sum_{i=1}^n \frac{\xi_i - \zeta_i}{\xi_i} \quad (6)$$

211

212 in which  $\xi_i$  and  $\zeta_i$  are the measurements for  $S_{oe} = 0\%$  and  $S_{oe} = 5\%$ , respectively, and  $n$  is the number  
213 of measurements. The comparisons show that  $y$  and  $h_M/h_0$  decrease in all cases with a radial bottom slope.  
214 This results is important evidence indicating that, by adding a radial bottom slope, it is possible to meet two  
215 seemingly conflicting design criteria, i.e., achieving a low  $y$  and low  $h_M/h_0$  at the same time.

216

Table 2 Changes in  $y$  and  $h_M/h_0$  according to the radial bottom slope

217

## 218 Conclusions

219

220 In this study, the performance of a spiral inlet, which is designed for a supercritical flow, was investigated  
221 experimentally in conditions of subcritical and transcritical flows. To prevent choking in the vertical shaft, a spiral  
222 intake structure with a guiding wall was installed. After varying the extent of the guiding wall and the longitudinal

223 and radial bottom slopes, water surface elevations were measured at a number of positions within the spiral inlet for  
224 different discharges. In all cases, choking was successfully prevented. Overall, a steeper longitudinal bottom slope  
225 reduces the water surface elevation at the beginning of the intake. However, a steeper bottom slope results in a  
226 transcritical flow in the intake structure, which causes the maximum water surface elevation to occur within the  
227 spiral intake. For effective design of a spiral inlet in subcritical and transcritical flows, achieving a low water surface  
228 elevation throughout the spiral intake structure is necessary; here, we experimentally showed that this can be  
229 achieved by using a radial bottom slope. Further work using model experiments and numerical simulations is  
230 underway to quantify the optimum design criteria by varying more various bottom slopes.

231

### 232 **Acknowledgement**

233 This study was supported by the grant (17CTAP-C095650-03) from Infrastructure and Transportation  
234 Technology Promotion Program funded by Ministry of Land, infrastructure, and Transport of Korean government  
235 and funded by the project ‘Development of Urban Flood Mitigation Technology (Smart Flood Management)’ of  
236 Korea Institute of Civil Engineering and Building Technology

237

### 238 **References**

- 239 1. Banisoltan S., Rajaratnam N., & Zhu D. Z. 2015 Experimental study of hydraulics of drill-drop manholes.  
240 *Journal of Hydraulic Engineering*, **141**(10), 04015021.
- 241 2. Crispino G., Dorthe D., Gisonni C., & Pfister M. 2016 Junction chamber at vortex drop shaft: case study of  
242 Cossonay. In: *Proceedings of the 6th IAHR Int. Symp. on Hydraul. Struct.*, Portland, OR, pp 437-446.
- 243 3. Drioli C. 1947 Su un particolare tipo d’imbocco per pozzi di scarico. *L’ Energia Elettrica*, **24**, pp. 447-452 (in  
244 Italian).
- 245 4. Del Giudice G. & Gisonni C. 2011 Vortex dropshaft retrofitting: case of Naples city (Italy). *Journal of*  
246 *Hydraulic Research*, **49** (6), pp. 804-808.
- 247 5. Del Giudice G., Gisonni C., & Rasulo G. 2010 Design of a scroll vortex inlet for supercritical approach flow.  
248 *Journal of Hydraulic Engineering*, **136** (10), pp. 837-841.
- 249 6. Hager W. H. 1985 Head-discharge relation for vortex shaft. *Journal of Hydraulic Engineering*, **111** (6), pp.  
250 1015–1020.

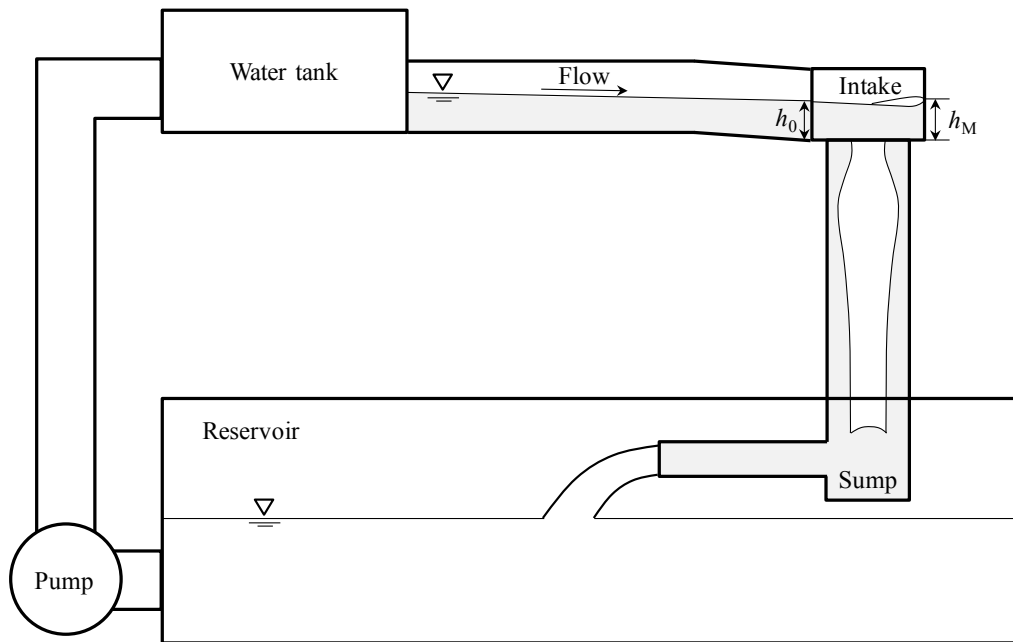
- 251 7. Hager W. H. 1990 Vortex drop inlet for supercritical approaching flow. *Journal of Hydraulic Engineering*, **116**  
252 (8), pp. 1048–1054.
- 253 8. Hager W. H. 2010 *Wastewater Hydraulics*, 2nd ed. Springer.
- 254 9. Ippen A. T. 1943 Gas-wave analogies in open channel flow. In: *Proceedings of the 2nd Hydraulic Conference*,  
255 Bulletin **27**, Studies in Engineering, University of Iowa.
- 256 10. Jain S. C. 1984 Tangential vortex-inlet. *Journal of Hydraulic Engineering*, **110** (12), pp. 1683-1699.
- 257 11. Jain S. C. & Kennedy J. F. (1983) Vortex-flow drop structures for the milwaukee metropolitan sewerage district  
258 inline storage system. *IIHR Report No. 264*, Iowa Institute Hydraulic Research, University of Iowa, Iowa City,  
259 Iowa.
- 260 12. Kellenberger M. H. 1988 *Wirbelfallschächte in der Kanalisationstechnik*, Doctoral dissertation, Swiss Federal  
261 Institute of Technology, Zurich, Switzerland (in German).
- 262 13. Motzet K. M. & Valentin F. 2002 Efficiency of a vortex chamber with horizontal bottom under supercritical  
263 flow. *Global Solutions for Urban Drainage*, ASCE, pp. 1-11.
- 264 14. Mulligan S., Casserly J., & Sherlock R. 2016 Effects of geometry on strong free-surface vortices in subcritical  
265 approach flows. *Journal of Hydraulic Engineering*, **142** (11), 04016051.
- 266 15. Rajaratnam N., Mainali A., & Hsung C.Y. 1997 Observations on flow in vertical dropshafts in urban drainage  
267 systems. *Journal of Hydraulic Engineering*, **123** (5), pp. 486-491.
- 268 16. Quick M. (1990) Analysis of spiral vortex and vertical slot vortex drop shafts. *Journal of Hydraulic*  
269 *Engineering*, **116** (3), pp. 309-325.
- 270 17. Wu J., Ren, W., & Ma F. 2017 Standing wave at dropshaft inlets. *Journal of Hydrodynamics*, **29** (3), pp.  
271 524-527.
- 272 18. Zhao C.H., Zhu D.Z., Sun S.K., & Liu Z.P. 2006 Experimental study of flow in a vortex drop shaft. *Journal of*  
273 *Hydraulic Engineering*, **132** (1), pp. 61-68.

Table 1 Summary of the experimental conditions

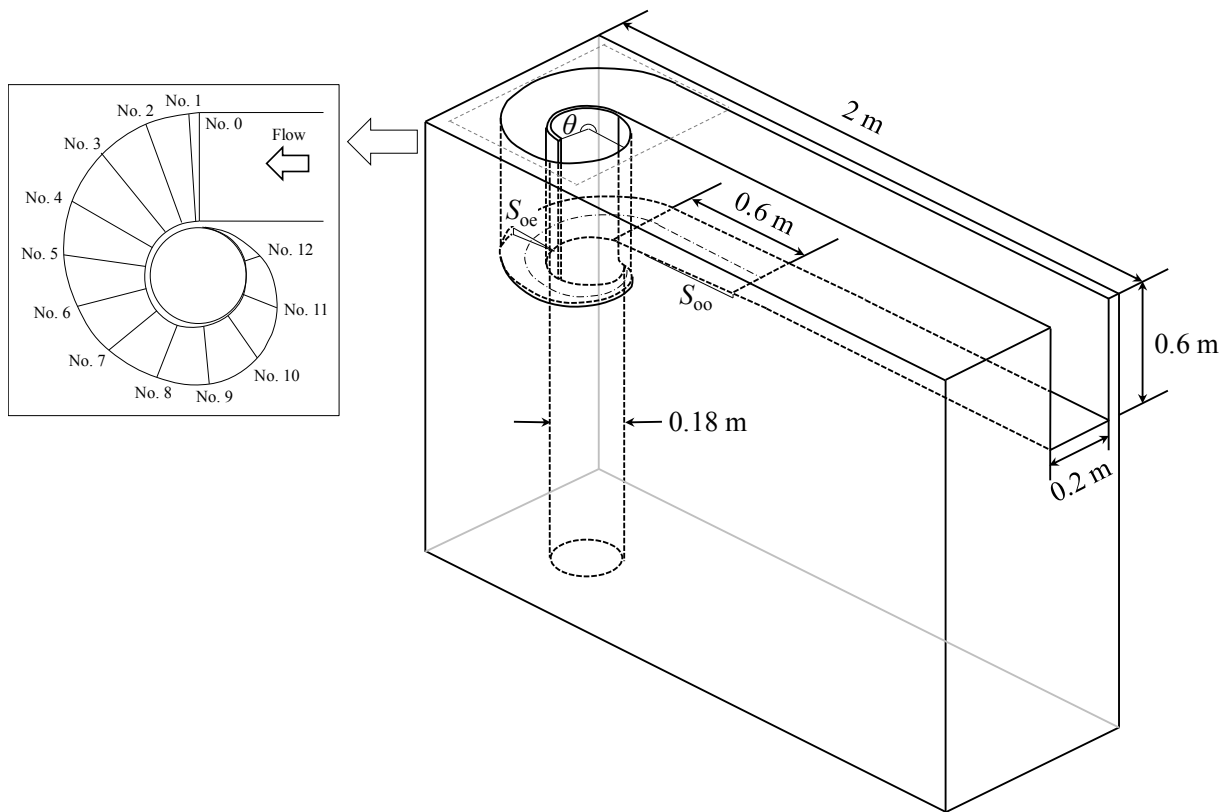
$Q$ (m <sup>3</sup> /s)	$\theta$ (°)	$S_{oe}$ (%)	$S_{oo}$ (%)	$F_o$	$q$
0.002 - 0.025	0 - 270	0.0	5.0	0.117-0.668	0.158-2.030
			7.5	0.137-1.129	
			10.0	0.188-1.129	
		5.0	12.5	0.175-1.218	
			5.0	0.162-1.202	
			10.0	0.207-1.247	

Table 2 Changes in  $\bar{y}$  and  $h_M/h_0$  according to the radial bottom slope

Case	$S_{oo} = 5\%$		$\varepsilon$ (%)	$S_{oo} = 10\%$		$\varepsilon$ (%)	
	$S_{oe} = 0\%$	$S_{oe} = 5\%$		$S_{oe} = 0\%$	$S_{oe} = 5\%$		
$\theta = 210^\circ$	$\bar{y}$	1.18	1.06	0.09	0.68	0.62	11.17
	$\overline{h_M/h_0}$	1.04	1.01	3.94	1.23	1.00	16.04
$\theta = 180^\circ$	$\bar{y}$	0.98	0.83	11.60	0.73	0.58	11.98
	$\overline{h_M/h_0}$	1.05	1.01	5.12	1.25	1.01	17.70
$\theta = 120^\circ$	$\bar{y}$	0.85	0.73	13.99	0.61	0.53	12.17
	$\overline{h_M/h_0}$	1.06	1.01	5.21	1.28	1.00	19.46
$\theta = 90^\circ$	$\bar{y}$	0.71	0.66	17.32	0.58	0.53	6.86
	$\overline{h_M/h_0}$	1.08	1.02	4.54	1.33	1.00	21.03



a) Outlines of experimental channel



b) Details of intake structures and measurement sections

Figure 1 Descriptions of the experimental apparatus

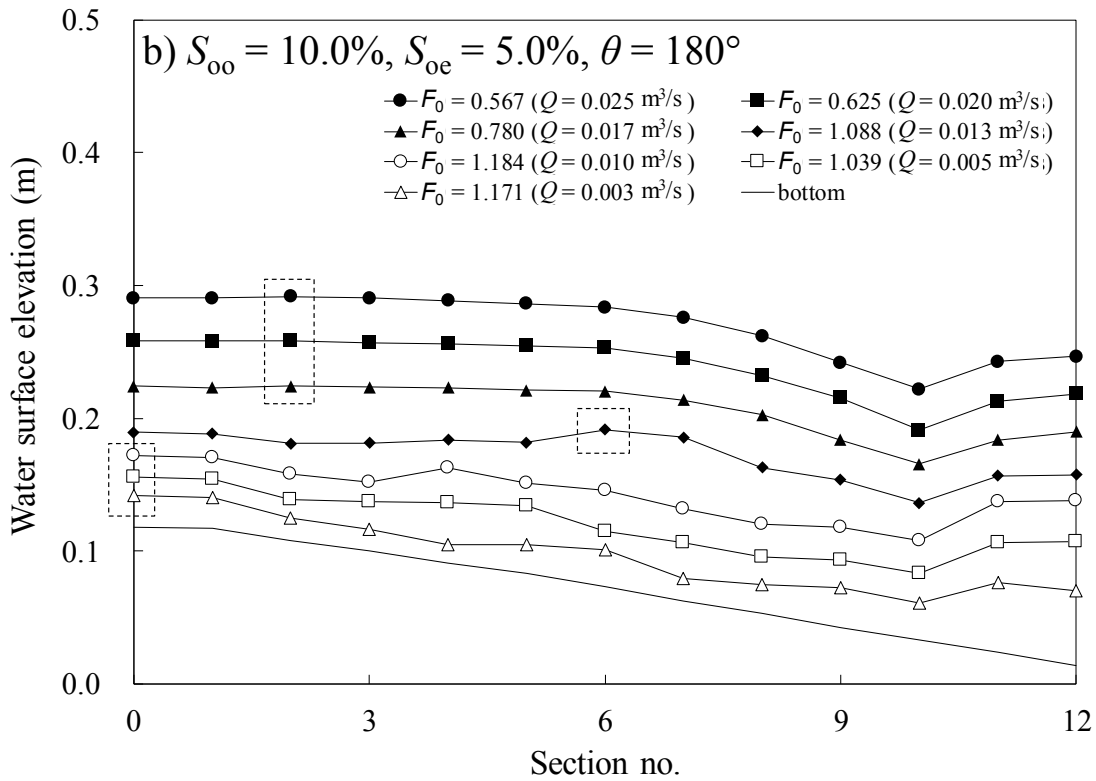
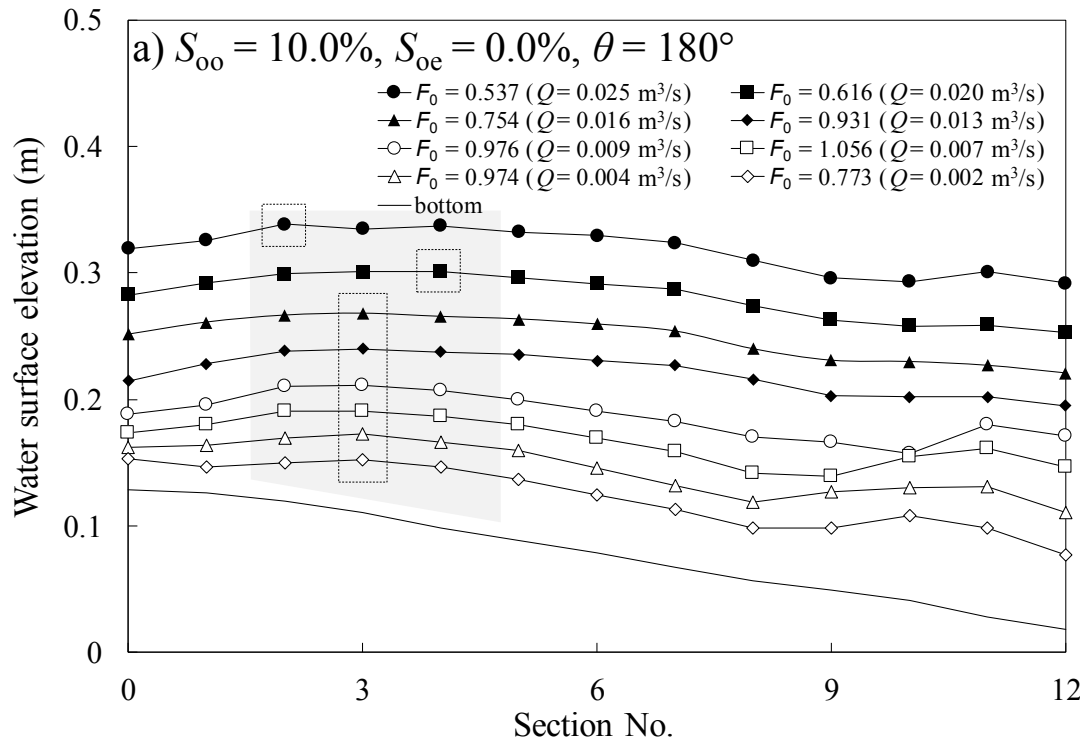


Figure 2 Experimental results for water surface elevations measured at intervals from the start of the spiral intake



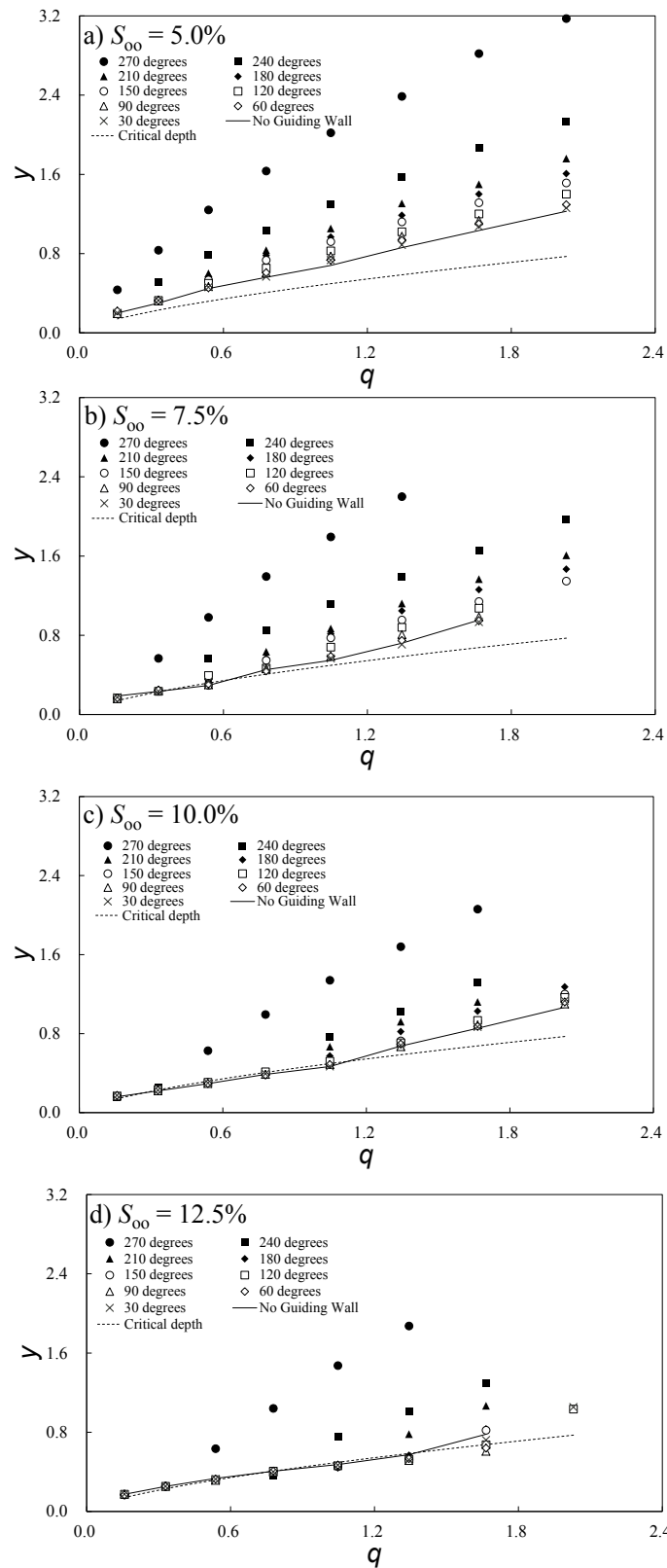


Figure 3  $y$  as function of  $q$  for the case with a longitudinal slope

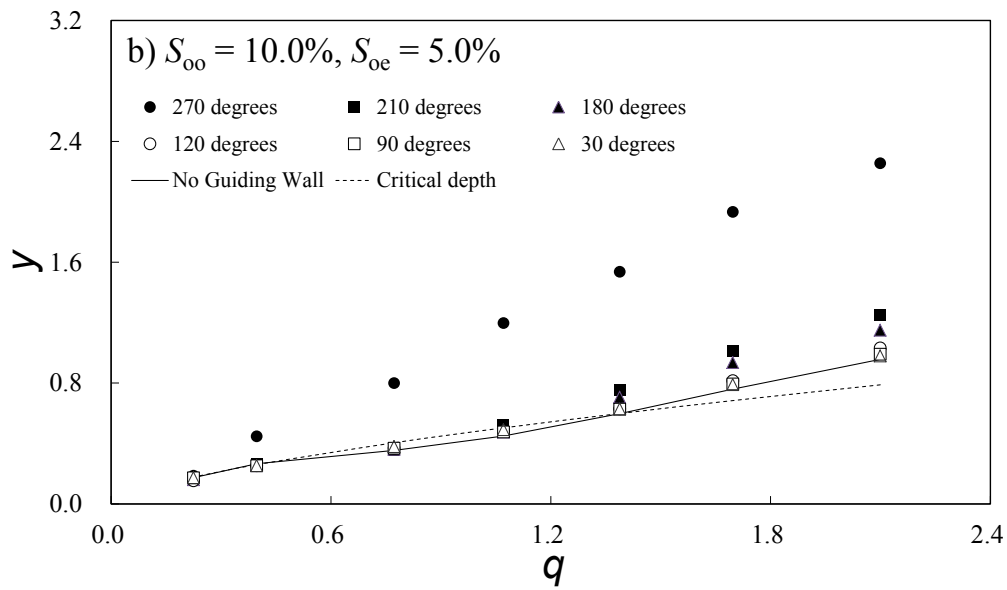
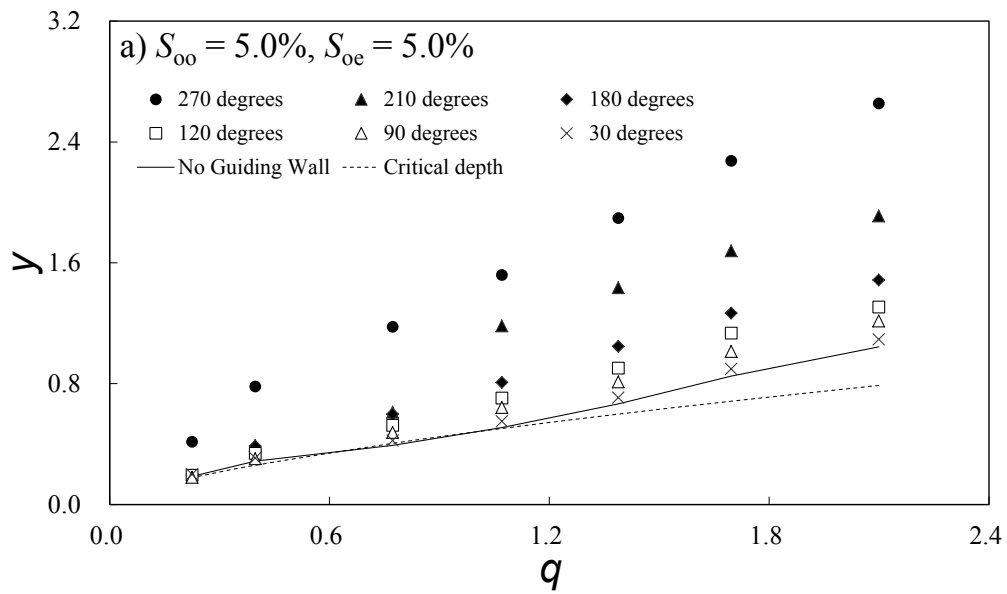


Figure 4  $y$  as a function of  $q$  for cases with longitudinal and radial slopes

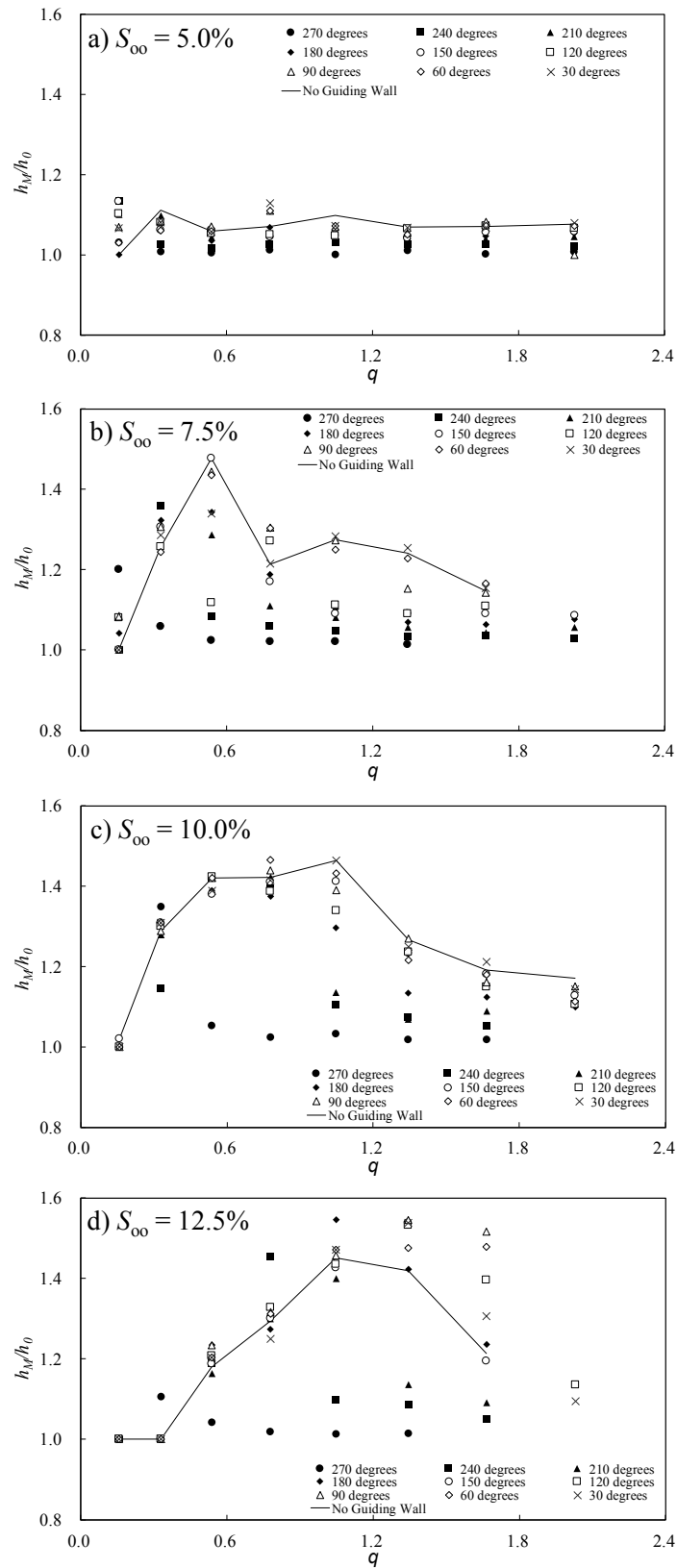


Figure 5  $h_M/h_0$  as a function of  $q$  for case with a longitudinal slope

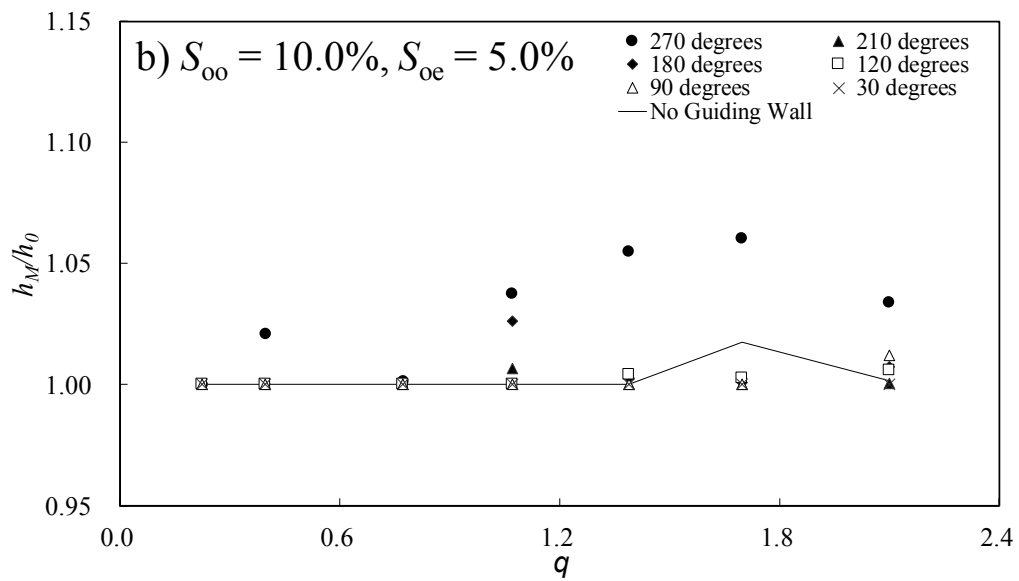
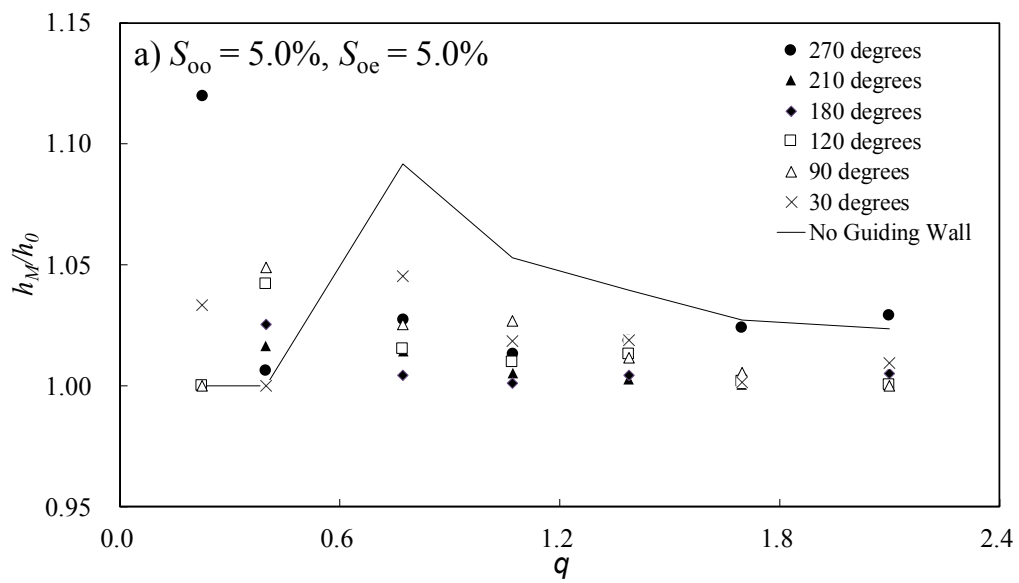


Figure 6  $h_M/h_0$  as function of  $q$  for cases with longitudinal and radial slopes

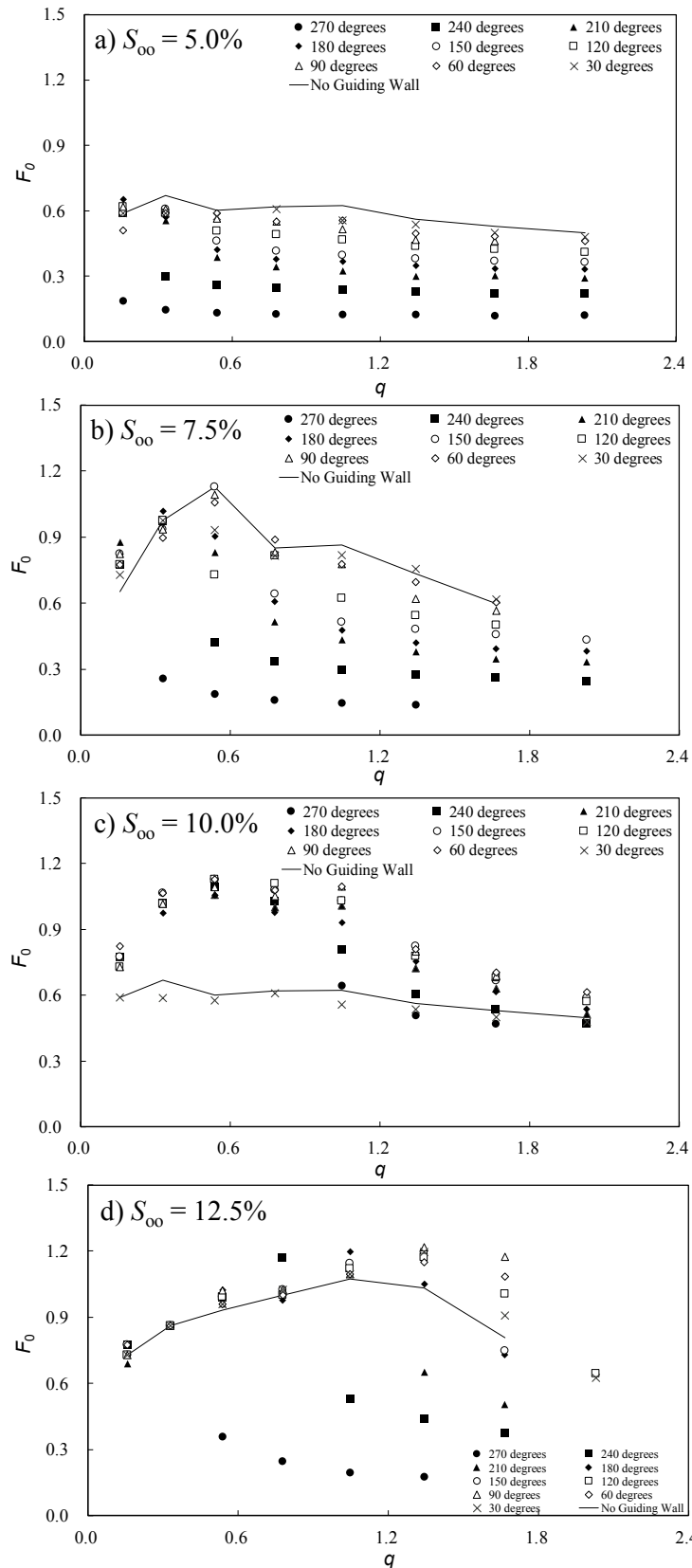


Figure 7  $F_0$  as a function of  $q$  for the case with a longitudinal slope

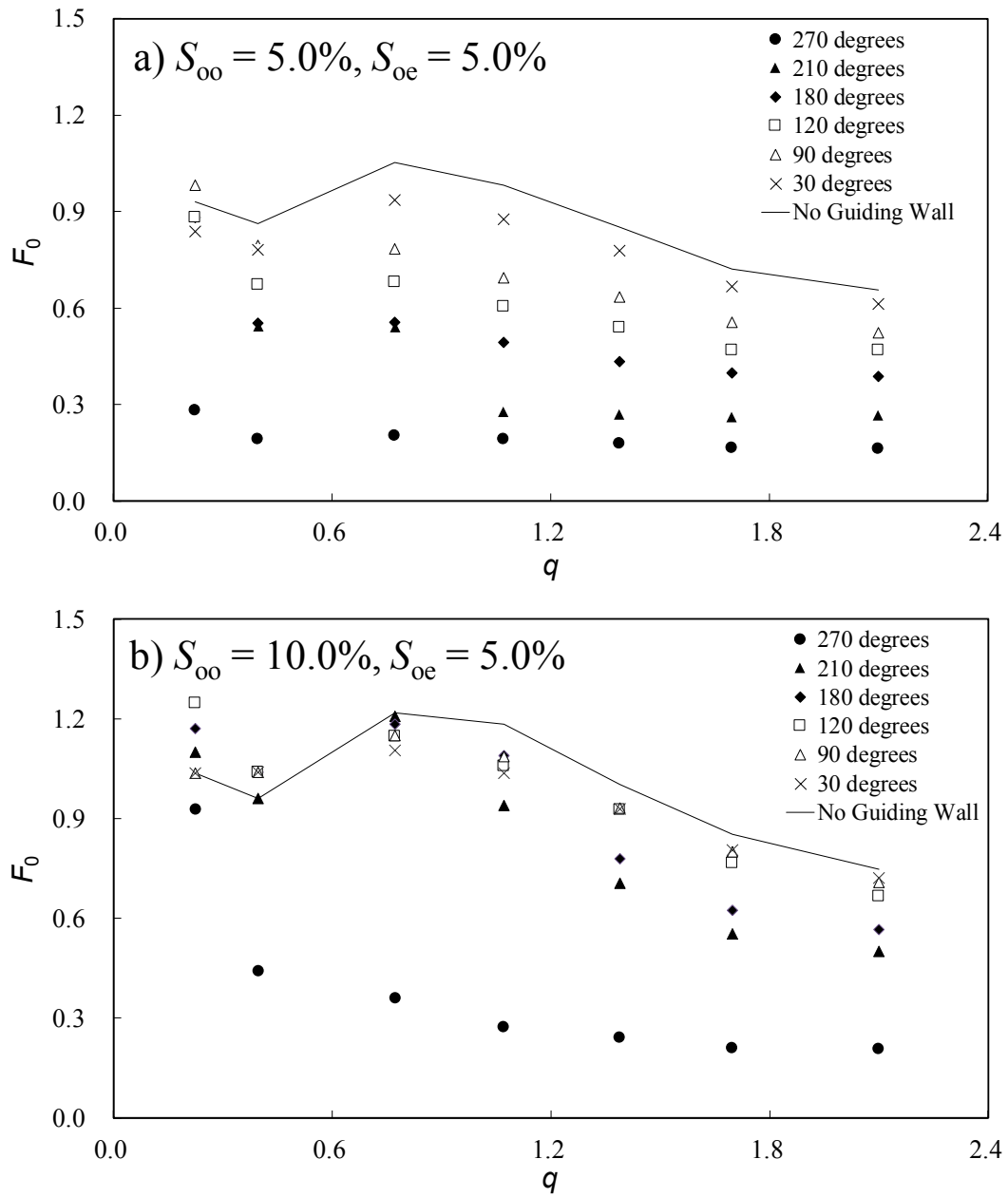
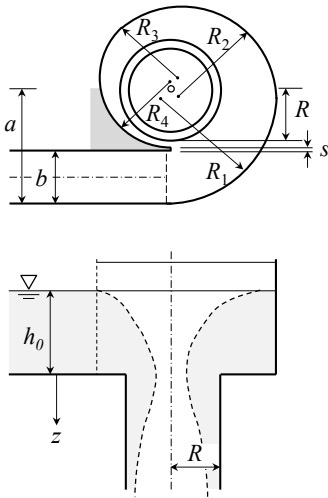
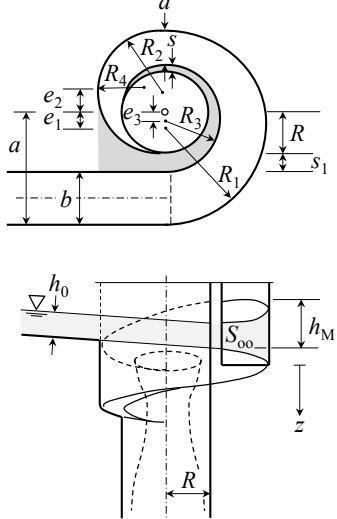


Figure 8  $F_0$  as a function of  $q$  for cases with longitudinal and radial slopes

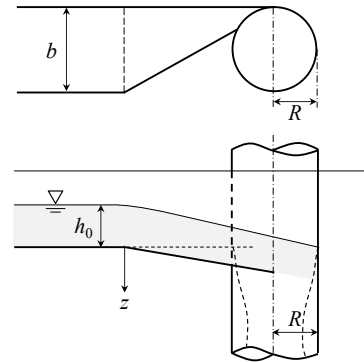
(a) Screw inlet



(b) Spiral inlet



(c) Tangential inlet



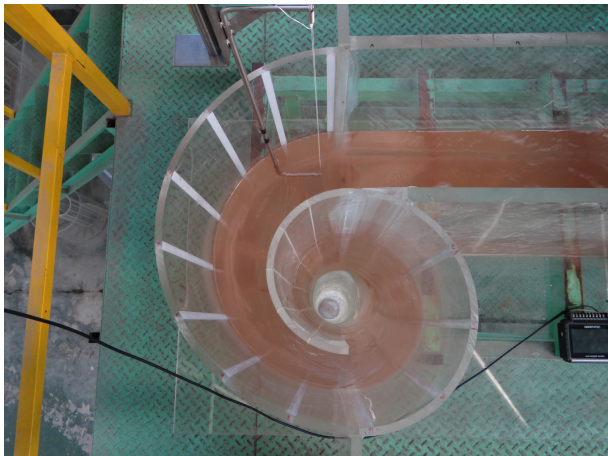
Appendix 1 Schematic diagrams for vortex drop inlets (adapted from Hager, 2010)



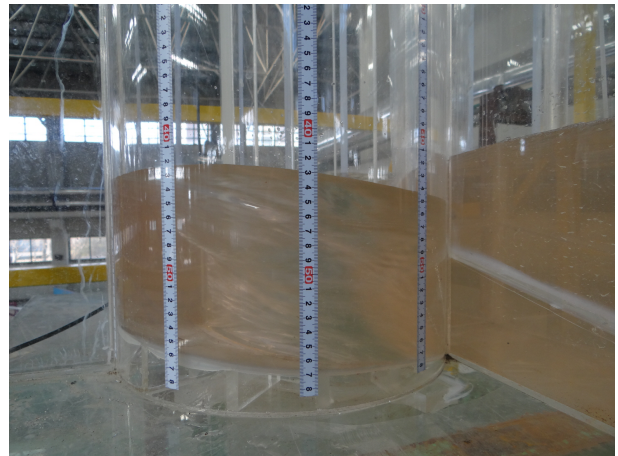
(a) Approach channel with the high-elevation tank



(b) Vertical shaft and outlet



(c) Top view of the vertical shaft with the spiral intake structure



(d) Tape rulers attached to the outer wall of the vertical shaft to measure water surface elevations

Appendix 2 Photographs of the model vortex drop inlet used in the experiments